Available online at www.sciencedirect.com
ScienceDirect
Trans. Nonferrous Met. Soc. China 24(2014) 2420−2426
Transactions of Nonferrous Metals Society of China
www.tnmsc.cn

Effect of cooling rate on morphology of primary particles in Al−Sc−Zr master alloy

Cong XU[1], Rou DU[1], Xue-jiao WANG[1], Shuji HANADA [2], Hiroshi YAMAGATA[3], Wen-hong WANG[4], Chao-li MA[1]

1. Key Laboratory of Aerospace Advanced Materials and Performance of Ministry of Education, School of Materials Science and Engineering, Beihang University, Beijing 100191, China;
2. Institute for Materials Research, Tohoku University, Sendai 980-8577, Japan;
3. Center for Advanced Die Engineering and Technology, Gifu University, 1-1 Yanagido, Gifu City, Gifu 501-1193, Japan;
4. Hebei Sitong New Metal Material Co., Ltd., Baoding 071105, China

Received 17 October 2013; accepted 30 April 2014

Abstract: Al−1.0%Sc−1.0%Zr (mass fraction) master alloy was prepared at different cooling rates. The morphology and thermodynamics data of the primary particles of the master alloy were investigated by X-ray diffraction (XRD), scanning electron microscopy (SEM) and differential scanning calorimetry (DSC). It shows that the primary particles are dendrite-shaped particles comprised of several attached small cubic, cusped-cubic or crucifer shape particles at slow cooling rate. However, the primary particles are separated with crucifer shape at intermediate cooling rate, and they are cubic with cusped-cubic shape at high cooling rate. Meanwhile, the separated and attached particles present $Al_3Sc/Al_3Zr_{1-x}Sc_x$ core-shell structure. The formation mechanism of the structure was systematically investigated by a mathematical model.

Key words: Al−Sc−Zr master alloy; morphology; core-shell structure; cooling rate; formation mechanism

1 Introduction

Optimizing the properties of alloy detailedly requires realizing not only the precipitation kinetics of its precipitates, but also the grain refinement of primary particles during solidification. However, the effect of adding distinct impurities to metal is not reduced to summing the effect of each of them. The addition of Zr and Sc elements to aluminum alloys is a prominent example [1]. Both elements increase the tensile strength and the recrystallization resistance of the alloy by forming ordered precipitates, respectively, but the combined effect of them is considerably larger, resulting from a higher density of smaller precipitates that are also less sensitive to coarsening [2−13]. This combined effect has been evaluated, and satisfactory explanation is available. CLOUET et al [14] elucidated the mechanism of the forming of precipitate core-shell structures by a broad range of experimental and computational techniques that allowed them to probe the particle formation and evolution process over length scales from the atomic to the micrometer. The precipitation kinetics of the precipitates in Al−Sc−Zr alloy has been evaluated in Ref. [15].

Optimizing the primary particles in master alloy was widely acknowledged as the cause of obtaining an alloy with high quality caused by precipitation strengthening and grain refinement [16]. However, few detailed observations of the morphology of the primary particles in Al−Sc−Zr master alloy at different cooling rates have been reported, and less formation mechanism of the core-shell structure in the master alloy was investigated. The main focus of this work was to explore the morphology of the primary particles and formation mechanism of the core-shell particles in Al−1.0%Sc−1.0%Zr master alloy at different cooling rates. In the end, Al−1.0%Sc−1.0%Zr master alloy was prepared by

Foundation item: Project (2012CB619503) supported by the National Basic Research Program of China; Project (2013AA031001) supported by the National High-tech Research and Development Program of China; Project (2012DFA50630) supported by the International Science and Technology Cooperation Program of China
Corresponding author: Chao-li MA; Tel: +86-10-82339772; E-mail: clma2001@gmail.com
DOI: 10.1016/S1003-6326(14)63366-5

vacuum melting method, and the extracted and sectioned particles in the master alloy were studied firstly. To better understand the formation mechanism of core-shell Al_3Sc/Al_3Zr structure in Al−Sc−Zr master alloy, a mathematical model of the formation of the particles was presented.

2 Experimental

The commercial Al−2.0%Sc (mass fraction) and Al−5.0%Zr master alloys were supplied as waffle ingot by Hebei Sitong New Metal Material Co., Ltd., China. Both master alloys, together with the commercial-purity (CP) aluminum (99.7%), were proportionally added into the JZ-IMT WZG-2 vacuum melting furnace for melting at (720±5) °C for 30 min. The melted alloy was cast into a wedge-shaped copper chill mould which produced the range of cooling rate between ~100 and ~1000 K/s [16] and small insulated alumina mould which produced the cooling rate of ~1 K/s. The compositions of commercial Al−Sc, Al−Zr and the Al−1.0%Sc−1.0%Zr master alloy prepared were analyzed by inductively coupled plasma atomic emission spectroscopy (ICP-AES), as shown in Table 1.

Table 1 Composition of commercial Al−Sc, Al−Zr and Al−Sc−Zr master alloys (mass fraction, %)

Sample	Sc	Zr	Impurity				Al
			Cu	Fe	Mg	Others	
Al−2.0%Sc	1.98	−	0.02	0.09	0.02	≤0.02	Bal.
Al−5.0%Zr	−	4.94	0.01	0.09	0.02	≤0.02	Bal.
Al−1.0%Sc−1.0%Zr	0.98	1.03	0.01	0.07	0.01	≤0.02	Bal.

The structure of the particles was determine as a function of the cooling rate, and metallographically polished section samples were taken from different positions along the centre line of each wedge casting, corresponding to different cooling rates. However, more Sc and Zr elements dissolve in aluminum matrix in the master alloy when the cooling rate was over 600 K/s, thus the primary particles were not almost found in the master alloy. Hence, the structure of the primary particles formed on solidification was studied in detail at three different cooling rates, namely, ~1, ~100 and 600 K/s (referred to slow, intermediate and high cooling rates, respectively). In addition, the primary particles were also extracted using a special extraction method [17]. The polished sections and extracted particles were examined by RIGAKU RINT-2000 X-ray diffractometer with Cu K_α radiation, CamScan Apollo300 field emission scanning electron microscope and NETZSCH STA 449 F3 Jupiter differential scanning calorimetry analyzer.

3 Results and discussion

3.1 Morphologies of primary particles in Al−Sc−Zr master alloy at different cooling rates

The XRD patterns of the extracted particles of Al−Sc−Zr master alloys at different cooling rates are shown in Fig. 1. It is found that all the master alloy ingots consist of α(Al), Al_3Sc and Al_3Zr phases at different cooling rates and there is no prominent change in the phases. HORI et al [18] suggested that the Al_3Zr particles present stable $D0_{33}$ Al_3Zr phase in Al−1.0%Zr alloy under the cooling rate of 100 K/s, metastable $L1_2$ phase contrarily. However, at cooling rate of ~1 K/s, most of Al_3Zr phase still forms the same structure of the Al_3Zr phase which forms at other cooling rates, metastable $L1_2$ lattice, contrasting with that of Al_3Zr phase, becomes $D0_{33}$ lattice in a binary Al−Zr alloy at this cooling rate.

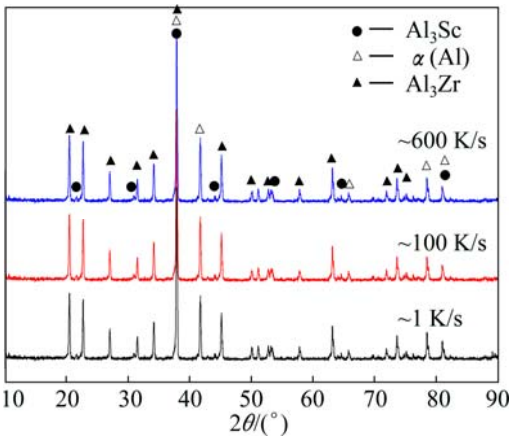

Fig. 1 XRD patterns of samples at different cooling rates

At high cooling rate (~600 K/s, at distance of 30 mm from the wedge tip), the morphology of the particles exhibits a cusped-cubic or cubic shape, as shown in Figs. 2(a) and (b), similar shaped particles have been observed in rapidly solidified Al−Zr [18,19] and Al−Hf [20] alloys. Most of the primary particles are separated because there is no enough time to congregate at high cooling rate. Meanwhile, core-shell $Al_3Sc/Al_3Zr_{1-x}Sc_x$ structure is found from line scan elements analysis (LSEA) of the particle, as shown in Fig. 2(c). KHARAKTEROVA et al [21] suggested that the shell has a smaller misfit (0.5%) with α(Al) compared to the $L1_2$ Al_3Sc phase (1.5%), which results in increasing the heterogeneous nucleation efficiency. This leads to cubic core-shell $Al_3Sc/Al_3Zr_{1-x}Sc_x$ structure of the separated primary particle. Meanwhile, a few small unstable particles grow along the ⟨111⟩ directions and exhibit cusped-cubic shape, caused by the destabilization of the particles. At intermediate cooling rate (~100 K/s, at the

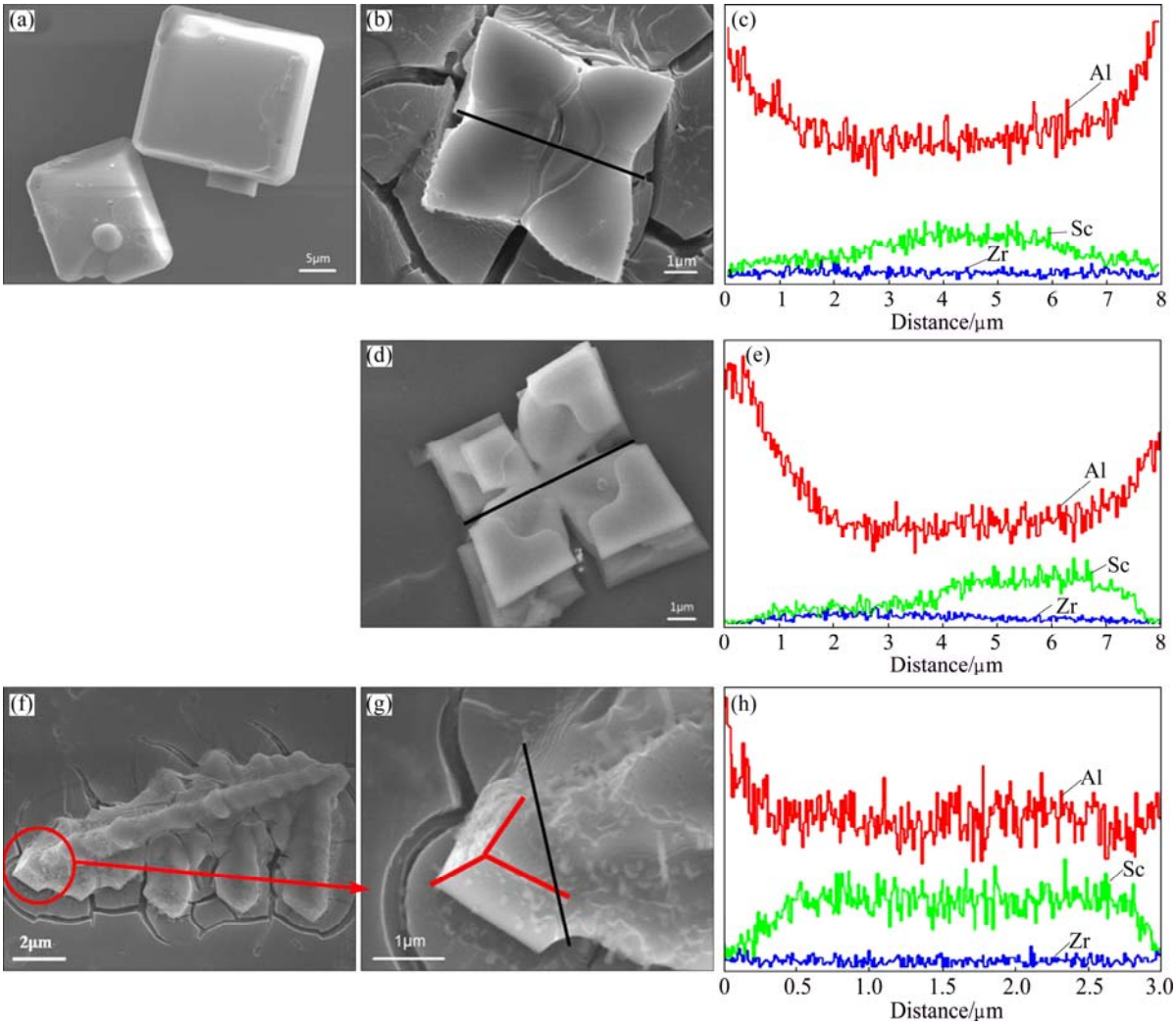

Fig. 2 SEM images and line scan elements analysis (LSEA) of particles extracted from samples at different cooling rates: (a, b, c) ~600 K/s, at distance of 30 mm from wedge tip; (d, e) ~100 K/s, at wedge top; (f, g, h) ~1 K/s, at small insulated alumina mould

top of the wedge), the primary particles exhibit crucifer shape and are separated by insufficient time to make them congregating at the cooling rate, as shown in Fig. 2(d). Meanwhile, it is found that the particles are core-shell $Al_3Sc/Al_3Zr_{1-x}Sc_x$ structure yet, as shown in Fig. 2(e). HYDE et al [22] suggested that the cubic particles must first develop by the growth of primary arms in the ⟨111⟩ directions, caused by some instability of the particles fading. Furthermore, the $Al_3Zr_{1-x}Sc_x$ shell still has the same structure of Al_3Sc core, $L1_2$ lattice, according to XRD analysis. Hence, crucifer shape particles appear resulting from some cusps growing along the eight corners of the cubic particle, and the core-shell $Al_3Sc/Al_3Zr_{1-x}Sc_x$ structure are not remodeled. At slow cooling rate (~1 K/s, the insulated alumina mould), there are enough time and energy to congregate the small particles for forming dendrite-shaped particles, as shown in Fig. 2(f). However, the LSEA of the small attached particles (Fig. 2(g)) shows that the particles are core-shell $Al_3Sc/Al_3Zr_{1-x}Sc_x$ structure yet. The XRD analysis shows that there is no prominent change of the structure in the attached particles, and the core-shell structure is not remodeled easily unless the structure of the shell changes.

The morphologies described above are the most common features observed at the three investigated cooling rates. The range of observations noted for a particular cooling rate, and changes in the structure within an individual particle during growth, are clearly related to variations in the local solidification conditions as the growing particles circulate in the melt. It is well known that phases with high entropy of fusion show a high growth rate anisotropy, which leads to the development of faceted structures. With such phases, growth occurs by the nucleation and migration of ledges across the solid-liquid interface [22]. When a small amount of Zr is added to Al−Sc alloy, the thermal stability of the alloy is improved. These effects can be attributed to the numerous substitutions of Sc atoms by Zr in the shell of $L1_2$ structure particles by forming the

Zr-rich shell during solidification [16]. The shell of $Al_3Zr_{1-x}Sc_x$ has slow-diffusing Zr and then acts as a barrier to the atomic transport that is required for particles to shrink if the others are to grow into larger particles, a process known as 'coarsening'. The shell therefore slows this coarsening process. The high number density of core-shell particles increases the strength and high-temperature creep resistance of the alloy, and the low coarsening rate gives rise to a high degree of thermal stability [14]. As a result, the master alloys with core-shell $Al_3Sc/Al_3Zr_{1-x}Sc_x$ structure have finer effect on aluminum alloy.

3.2 Formation of core-shell $Al_3Sc/Al_3Zr_{1-x}Sc_x$ structure

Based on FEG-SEM images and LSEA of the single particles (including the small attached particles in the dendrite-shape particles) extracted from the samples at different cooling rates, in the interior of single smaller particles in all master alloys, the shell of $Al_3Zr_{1-x}Sc_x$ phase surrounds the Al_3Sc core, leading to the formation of core-shell structure. CLOUET et al [23] elucidated the mechanism of how the precipitate core-shell structures form in Al−Sc−Zr alloy using a broad range of experimental and computational techniques that allowed them to probe the particle formation and evolution process over length scales from the atomic to the micrometer. The simulations and experiments point to novel nucleation and growth mechanism of the precipitates, with Zr playing a crucial role in both processes. Meanwhile, a spherical model treats cubic, similar to cubic or equiaxed particles and may therefore make realistic predictions inside the limits of its applicability [24]. As a result, the formation process of the core-shell $Al_3Sc/Al_3Zr_{1-x}Sc_x$ structure in the master alloy in detail can be modeled, as shown in Fig. 3. With temperature decreasing, Sc and Zr begin to congregate in melting alloy, and Al_3Sc phase forms earlier after the nuclei are formed, the particles grow by primarily absorbing Sc, because diffusivity of Sc is very larger than Zr [25]. Just after the formation of globular Al_3Sc phase, some cluster of Zr with smaller diffusivity is left to surround spontaneously onto Al_3Sc phase to minimize the surface energy [26]. This leads to the formation of core-shell $Al_3Sc/Al_3Zr_{1-x}Sc_x$ structure. This result is further confirmed by the DSC curve of the master alloy at the cooling rate of ~1 K/s, as shown in Fig. 4. Dissolution occurs on the interface among the smaller attached particles in the dendrite-shape particles at 714 °C, and then the particles begin dispersing themselves from the dendrite-shape particles body. When the temperature reaches 806 °C, the $Al_3Zr_{1-x}Sc_x$ shell begins dissolving, and the Al_3Sc core dissolves generally over 979 °C. Consequently, Al_3Sc phases which form firstly caused by bigger diffusivity of the Sc in melting aluminum alloy are spontaneous to agglomerate together to minimize the surface energy. In this case, $Al_3Zr_{1-x}Sc_x$ phase, which enwraps the Al_3Sc phase around, functions as a potent protective shell to lower the free energy of Al_3Sc and preclude the S/L interface from moving further, inhibiting the conglomeration and growth of Al_3Sc phases significantly.

3.3 Mathematical model of formation of core-shell $Al_3Sc/Al_3Zr_{1-x}Sc_x$ structure

WANG et al [27] investigated systematically the formation mechanism of core-shell $TiAl_3/Ti_2Al_{20}Ce$ in melt-spun Al−Ti−B−RE grain refiner by a mathematical model based on Jander's equation. Similarly, the formation of core-shell structure could be also simplified as a mathematical model in Fig. 5, however, the model based on Gentling equation, which abandons the assumption of constant diffusion section in Jander's equation, illuminates dynamics of core-shell diffusion better. As the $Al_3Zr_{1-x}Sc_x$ shell grows, the radius of Al_3Sc core decreases and the layer of Zr gets attenuated correspondingly. The formative kinetics of $Al_3Zr_{1-x}Sc_x$ shell could conform to Gentling equation which is written as follows:

$$1-\frac{2}{3}G-(1-G)^{\frac{2}{3}}=K_J t \tag{1}$$

where G is the volume fraction of Zr layer converted to $Al_3Zr_{1-x}Sc_x$ shell, K_J is the Gentling rate constant and t is the time. K_J could be written as

$$K_J=\frac{2K}{R_0^2} \tag{2}$$

where K is the rate constant related with temperature T, diffusion coefficient D and contact conditions; R_0 (in Fig. 5) is the radius of the $Al_3Sc/Al_3Zr_{1-x}Sc_x$ spherical particle. Solving hereinbefore equations simultaneously

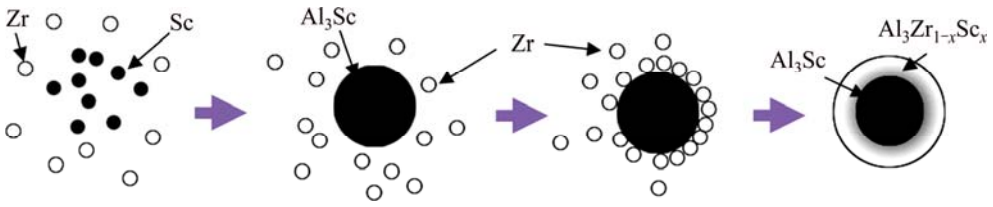

Fig. 3 Schematic diagram of formation of single small particle in Al−Sc−Zr master alloy

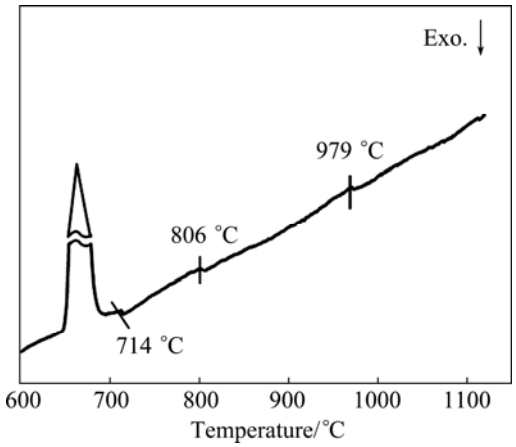

Fig. 4 DSC curve of Al−Sc−Zr master alloy at cooling rate of ~1 K/s

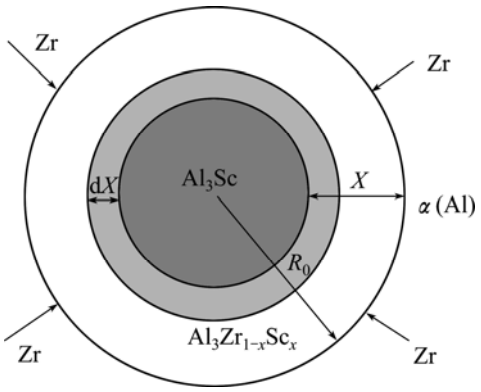

Fig. 5 Mathematical model of formation of core-shell $Al_3Sc/Al_3Zr_{1-x}Sc_x$ structure

as follows:

$$[1-\frac{2}{3}G-(1-G)^{\frac{2}{3}}]\cdot R_0^2=2Kt \tag{3}$$

It is assumed that the growth rate of Al_3Zr shell is inversely proportional to the time of shell growth t as

$$\frac{dX}{dt}=\frac{K}{1+t} \tag{4}$$

where X (in Fig. 5) is the thickness of $Al_3Zr_{1-x}Sc_x$ shell. Integrating both sides of Eq. (4) gives

$$X=K\ln(1+t) \tag{5}$$

The shell grows up quickly during solidification, $\ln(1+t)$ is approximately equal to t when t is small. As a result, the change of Eq. (5) gives

$$X=K\cdot t \tag{6}$$

The X is set as function of volume fraction G, which can be obtained according to Eqs. (3) and (6)

$$[1-\frac{2}{3}G-(1-G)^{\frac{2}{3}}]\cdot R_0^2=2X \tag{7}$$

As shown in Eq. (7), X is proportional to R_0 and G. According to Figs. 2(c, e, h), both R_0 and X of three samples at different cooling rate (~1, ~100 and 600 K/s) can be determined approximately and their sizes are in the order of 1.25 μm and 0.3 μm, 2.0 μm and 1.00 μm, 1.5 μm and 1.00 μm, respectively. From Eq. (7), it is seen that G is a function of X and R_0. In view of that, the conversion rate of $Al_3Zr_{1-x}Sc_x$ shell could be calculated. At cooling rate of ~1, ~100, and ~600 K/s, G is 0.991, 0.976 and 0.792, respectively. It is concluded that the conversion rates of $Al_3Zr_{1-x}Sc_x$ shell of the single particle or the small attached particle decrease with the cooling rate increasing and instantly reach an extreme platform below the cooling rate of ~100 K/s. Many Refs. [2,4,5,7] illustrated the kinetics of the diffusion process obviously plays an important role in the development of the core-shell precipitates. At high cooling rare (~600 K/s), parts of Sc atoms form instantly the core of core-shell structure as the speedy diffusion of Sc atoms, but parts of Zr atoms, playing a crucial role in both processes, are left to precipitate on the Sc core, creating the shell in the matrix. The other particles of Sc and Zr atoms are dissolved in α(Al) matrix. The G value (0.792) of the sample, based on the mathematical model, basically reflects small diffusivity of Zr atoms at this cooling rate. Segregation of Zr atoms to the shell around the core thus reduces the misfit with the Al matrix quickly (form 1.5% to 0.5%) and only a small amount of Zr atoms can form the shell [28]. It is possible that the G value of the sample at the cooling rates is still over 50%, although the diffusivity of Zr atoms is interfered by the cooling rate. At lower cooling rates (~1 K/s or ~100 K/s), Sc atoms have enough time to form the core in core-shell particles, and slower-diffusing Zr atoms are left to create the shell. The higher G values (0.976 and 0.991) of two samples reflect similarly the larger diffusivity of Zr atoms at lower cooling rates.

4 Conclusions

1) At high cooling rate (~600 K/s), the morphology of the particles exhibits a cusped-cubic or cubic shape. Most of the primary particles form core-shell $Al_3Sc/Al_3Zr_{1-x}Sc_x$ structure and are separated resulting from no enough time to congregate at high cooling rate. At intermediate cooling rate (~100 K/s), the primary particles present crucifer shape and are still separated, which is caused by insufficient time to make them congregating at the cooling rate, meanwhile, the core-shell $Al_3Sc/Al_3Zr_{1-x}Sc_x$ structure is found yet. At slow cooling rate (~1 K/s), there are enough time and energy to congregate the small cube-shaped, cusped-cubic shape or crucifer-shaped particles for forming dendrite-shaped particles, and the attached particles are

core-shell $Al_3Sc/Al_3Zr_{1-x}Sc_x$ structure.

2) The formation mechanism of the core-shell $Al_3Sc/Al_3Zr_{1-x}Sc_x$ structure was investigated by mathematical model. The conversion rate of $Al_3Zr_{1-x}Sc_x$ shell could be calculated. At cooling rates of ~1, ~100 and ~600 K/s, G is 0.991, 0.976 and 0.792, respectively. It is concluded that the conversion rates of $Al_3Zr_{1-x}Sc_x$ shell of the single particle or the small attached particle decease with the cooling rate increasing and instantly reach an extreme platform below the cooling rate of ~100 K/s. This is mainly related to the diffusion of Sc and Zr atoms in the master alloy at different cooling rates.

References

[1] VOORHEES P W. Alloy: Scandium overtakes zirconium [J]. Nature Materials, 2006, 5: 435−436.

[2] YELAGIN V I, ZAKHAROV V V, PAVLENKO S G, ROSTOVA T D. Influence of zirconium additions on ageing of Al−Sc alloys [J]. Physics of Metals and Metallography, 1985, 60 (1): 88−92.

[3] DAVYDOV V G, YELAGIN V I, SAKHAROV V V, ROSTOVA T D. Alloying aluminum alloys with scandium and zirconium additives [J]. Metal Science and Heat Treatment, 1996, 38(8): 347−352.

[4] ZOU Liang, PAN Qing-lin, HE Yun-bin, WANG Chang-zhen, LIANG Wen-jie. Effect of minor Sc and Zr addition on microstructures and mechanical properties of Al−Zn−Mg−Cu alloys [J]. Transactions of Nonferrous Metals Society of China, 2007, 17(2): 340−345.

[5] FULLER C B, SEIDMAN D N, DUNAND D C. Mechanical properties of Al(Sc,Zr) alloys at ambient and elevated temperatures [J]. Acta Materialia, 2003, 51(16): 4803−4814.

[6] DANG Jing-zhi, HUANG Yu-feng, CHENG Jun. Effect of Sc and Zr on microstructures and mechanical properties of as-cast Al−Mg−Si−Mn alloys [J]. Transactions of Nonferrous Metals Society of China, 2009, 19(3): 540−544.

[7] MENG Yi, ZHAO Zhi-hao, CUI Jian-zhong. Effect of minor Zr and Sc on microstructures and mechanical properties of Al−Mg−Si−Cu−Cr−V alloys [J]. Transactions of Nonferrous Metals Society of China, 2013, 23(7): 1882−1889.

[8] DENG Y, XU G. F, YIN Z M, LEI LEI X F, HUANG J W. Effects of Sc and Zr microalloying additions on the recrystallization texture and mechanism of Al−Zn−Mg alloys [J]. Journal of Alloys and Compounds, 2013, 580: 412−426.

[9] JIA Zhi-hong, RØYSET J, SOLBERG J K, LIU Qing. Formation of precipitates and recrystallization resistance in Al−Sc−Zr alloys [J]. Transactions of Nonferrous Metals Society of China, 2012, 22(8): 1866−1871.

[10] DUAN J Q, YIN Z M, ZHAO K, DENG Y, LEI X F. Microstructure evolution and $Al_3(Sc_{1-x}Zr_x)$ precipitates' kinetics in Al−Zn−Mg alloy during homogenization [J]. Journal of Central South University, 2013, 20(3): 579−586.

[11] FULLER C B, SEIDMAN D N. Temporal evolution of the nanostructure of Al(Sc,Zr) alloys: Part II-Coarsening of $Al_3(Sc_{1-x}Zr_x)$ precipitates [J]. Acta Materialia, 2005, 53(20): 5415−5428.

[12] RIDDLE Y W, SANDERS T H. A study of coarsening, recrystallization and morphology of microstructure in Al−Sc−(Zr)−(Mg) alloys [J]. Metallurgical and Materials Transactions A, 2004, 35(1): 341−350.

[13] TOROPOVA L S, ESKIN D G, KHRATEROVA M L, BOBATKINA T V. Advanced aluminum alloys containing Scandium—Structure and properties [M]. Newark, NJ: Gordon and Breach Sciences Publishers, 1999.

[14] CLOUET E, NASTAR M, SIGLI C. Nucleation of Al_3Zr and Al_3Sc in aluminum alloys: From kinetic monte carlo simulations to classical theory [J]. Physical Review B, 2004, 69(6): 064109−064123.

[15] LAI J, ZHANG Z, CHEN X G. Precipitation strengthening of Al−B_4C metal matrix composites alloyed with Sc and Zr [J]. Journal of Alloys and Compounds, 2013, 552(5): 227−235.

[16] NOMAN A F, PRANGNELL P B, MCEWEN R S. The solidification behavior of dilute aluminum−scandium alloys [J]. Acta Materialia, l998, 46(16): 5715−5732.

[17] LIU C P, PAN F S, WANG W Q. Phase analysis of Al−Mn compounds in the AZ magnesium alloys [J]. Materials Science Forum, 2007, 546−549(1): 395−398.

[18] HORI S, SAJI S, TAKEHARA A. Structure of rapidly solidified Al−Zr alloys and its thermal stability [C]//Prco. 4th Int Conf on Rapidly Quenched Metals. Sendi, Japan, 1981: 1538−1545.

[19] HORI S, UNIGAME Y, FURUSHIRO N, TAI H. Phase decomposition in splat quenched Al−6%Hf alloy [J]. Journal of Japan Institute of Light Metals, 1982, 32: 408−412.

[20] NOMAN A F, TSAKIROPOULOS P. The microstructure and properties of rapidly solidified Al−Hf alloys[J]. Materials Science and Engineering A, 1991, 134(25): 1144−1147.

[21] KHARAKTEROVA M L, ESKIN D G, TOROPOVA L S. Precipitation hardening in ternary alloys of the Al−Sc−Cu and Al−Sc−Si systems [J]. Acta Metallurgica et Materialia, 1994, 42(7): 2285−2290.

[22] HYDE K B, NOMAN A F, PRANGNELL P B. The effect of cooling rate on the morphology of primary Al_3Sc intermetallic particles in Al−Sc alloys [J]. Acta Materialia, 2001, 49(8): 1327−1337.

[23] CLOUET E, LAÉ L, ÉPICIER T, LEFEBVRE W, NASTAR M, DESCHAMPS A. Complex precipitation pathways in multi-component alloys [J]. Nature Materials, 2006, 5(6): 482−488.

[24] GREER A L, BUNN A M, TRONCHE A, EVANS P V, BRISTOW D J. Modelling of inoculation of metallic melts: application to grain refinement of aluminium by Al−Ti−B [J]. Acta Materialia, 2000, 48(11): 2823−2835.

[25] FUJIKAWA S I. Impurity diffusion of scandium in aluminum [J]. Defect and Diffusion Forum, 1997, 143: 115−120.

[26] ZHAO H L, SONG Y, LI M, GUAN S K. Grain refining efficiency and microstructure of Al−Ti−C−RE master alloy [J]. Journal of Alloys and Compounds, 2010, 508(1): 206−211.

[27] WANG K, CUI C X, WANG Q, LIU S J, GU C S. The microstructure and formation mechanism of core-shell-like $TiAl_3/Ti_2Al_{20}Ce$ in melt-spun Al−Ti−B−Re grain refiner [J]. Materials Letters, 2012, 85(15): 153−156.

[28] TOLLEY A, RADMILOVIC V, DAHMEN U. Segregation in $Al_3(Sc,Zr)$ precipitates in Al−Sc−Zr alloys [J]. Scripta Materialia, 2005, 52(7): 621−625.

冷却速率对 Al−Sc−Zr 中间合金中初始粒子形貌的影响

徐 聪[1]，杜 柔[1]，王雪姣[1]，Shuji HANADA[2]，Hiroshi YAMAGATA[3]，王文红[4]，马朝利[1]

1. 北京航空航天大学 材料科学与工程学院，空天先进材料与服役教育部重点实验室，北京 100191；
2. Institute for Materials Research, Tohoku University, Sendai 980-8577, Japan；
2. Center for Advanced Die Engineering and Technology, Gifu University,
1-1 Yanagido, Gifu City, Gifu 501-1193, Japan；
4. 河北四通新型金属材料股份有限公司，保定 071105

摘 要：在不同的冷却速率下制备 Al−1%Sc−1%Zr 中间合金。通过 X 射线衍射仪(XRD)、扫描电子显微镜 (SEM)和差示扫描量热仪 (DSC) 对中间合金初生粒子形貌和热力学性质进行研究。结果表明：初生粒子在低冷却速率时，是由一些立方、尖立方或十字花状的小粒子粘结组成的枝晶状颗粒。但是，初生粒子在中等的冷却速率时呈现分散的十字花状，在高冷却速率时呈现分散的立方状。不同冷却速率下十字花状和立方状单个粒子以及枝状晶中粘附粒子呈现 Al_3Sc/Al_3Zr 核−壳结构。通过数学模型对该结构的形成机制进行研究。

关键词：Al−Sc−Zr 中间合金；形貌；核−壳结构；冷却速度；形成机制

(Edited by Chao WANG)